

www.acsami.org Research Article

Highly Distorted Grain Boundary with an Enhanced Carrier/Phonon Segregation Effect Facilitates High-Performance Thermoelectric Materials

Shuankui Li, Zhongyuan Huang, Rui Wang, Wenguang Zhao, Jun Luo, Yinguo Xiao,* and Feng Pan*



Cite This: ACS Appl. Mater. Interfaces 2021, 13, 51018–51027



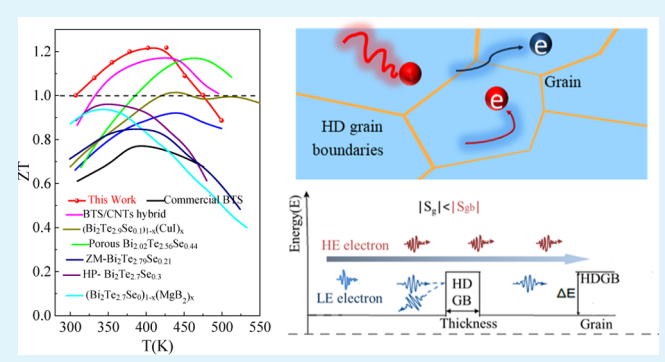
ACCESS

III Metrics & More

Article Recommendations

s Supporting Information

ABSTRACT: Grain boundary plays an important role in determining the phonon/carrier transport behaviors of thermoelectric (TE) materials, especially for the polycrystalline materials with the average grain size in nanoscale dimensions. Adjusting the grain size and boundaries of TE materials is considered as an effective approach to decouple TE parameters and thereby synergistically optimize the TE performance. Here, the highly distorted grain boundary with an enhanced carrier/phonon segregation effect is introduced to the commercial n-type Bi₂Te_{2.7}Se_{0.3} matrix. The existence of highly distorted grain boundaries can not only enhance the interfacial Seebeck coefficient without significant detriment to the electrical conductivity but also increase the interfacial thermal resistance of grain boundaries,



leading to the synergistic reduction of the thermal conductivity. As a result, a peak figure of merit $zT_{\rm max}\approx 1.22@425$ K and an average $zT_{\rm avg}\approx 1.1(300-500$ K) are obtained, which are about 55 and 57% higher than the corresponding values of the commercial Bi₂Te_{2.7}Se_{0.3} matrix, respectively. This work represents a new avenue for improving the commercial Bi₂Te_{2.7}Se_{0.3} TE material, which could further promote the development of the TE technology.

KEYWORDS: thermoelectric, Bi₂Te_{2.7}Se_{0.3}, hot deforming, grain boundary, defects

1. INTRODUCTION

As a promising green energy technology enabled direct conversion between electricity and heat, thermoelectric (TE) energy harvesting has been widely studied during the past decades due to its widespread application potential in space exploration, microelectronics, solid-state refrigeration, and so on.3 However, the low TE conversion efficiency limits its widespread application, which depends on the dimensionless figure of merit, $zT = S^2 \sigma T / \kappa$, where T, S, σ , and κ are the absolute temperature, the Seebeck coefficient, the electrical conductivity, and the total thermal conductivity (including both the lattice contribution κ_{latt} and the carrier contribution $\kappa_{\rm e}$), respectively. ⁴⁻⁶ The key factor hindering the enhancement of the zT value is the strong interrelation between σ , S, and κ . The core idea in development of TE materials is synergistic modulation of the coupled thermal and electrical transport properties.⁷ Despite the limited reports, grain boundary engineering has been proved to be an effective route to realize the synergistic modulation of charge carriers and phonon transport. However, successful implementation of this approach remains challenging because it is difficult to design the microstructure, chemical components, and thickness of grain boundaries at the atomic scale.

As an effective route to decouple the carrier and phonon transport, grain boundary engineering mainly related the energy flitting effect to balance the electrical transport performance and thermopower as well as the phonon scattering effect to reduce the lattice thermal transport performance.8 To maximize the effects of grain boundary, careful attention should be paid to weigh the effects on carrier/ phonon transport properties. For the carrier transport, the energy barrier at the grain boundary could block the lowenergy carriers, resulting in an increased thermopower. Meanwhile, the grain boundaries may also serve as phonon scattering centers to reduce the κ_{latt} , which is the so-called thermal interface resistance. However, in the real TE bulk, the grain boundaries usually act as the scattering centers of both the carrier and phonon, which result in the high interfacial thermal resistance as well as electrical resistance. 10-12 Design-

Received: August 12, 2021 Accepted: October 14, 2021 Published: October 26, 2021





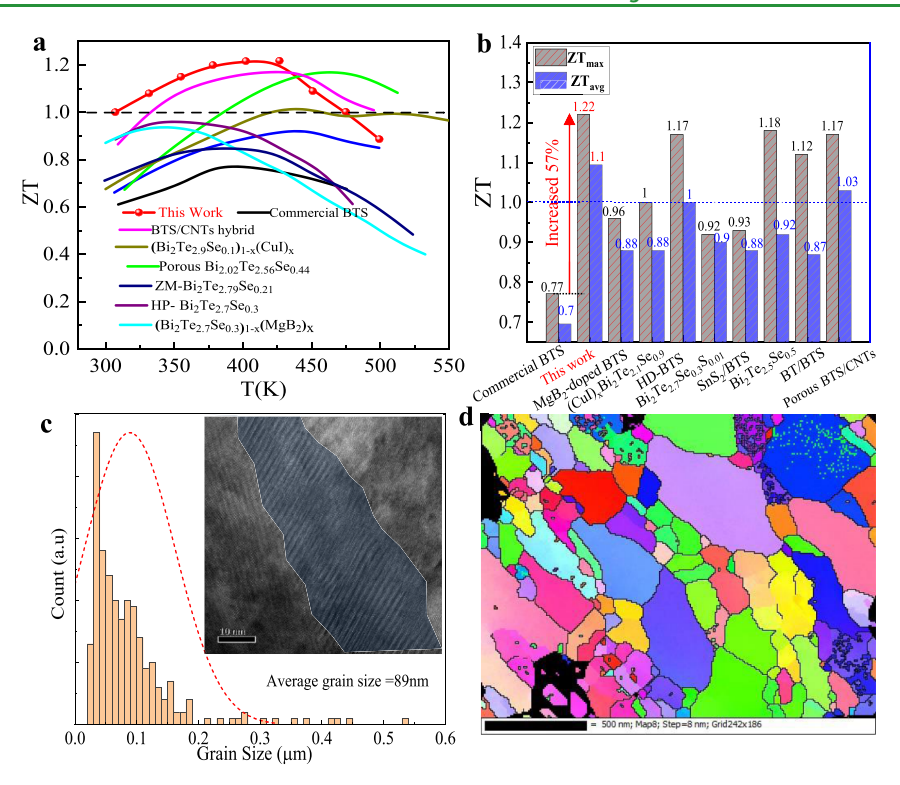


Figure 1. (a) Temperature-dependent zT and (b) maximum and average zT values for the as-prepared sample, including a comparison to the available reference. (c) Size distribution of grains and (d) corresponding EBSD maps of the as-prepared sample; the inset of (c) is the typical TEM image for the highly distorted grain boundary.

ing grain boundaries with an enhanced carrier/phonon segregation effect, in which the phonon scattering effect could be enhanced without the influence on the carrier transport, finally leads to a large net enhancement of zT. In practice, there are only few successful demonstrations of simultaneously increasing the thermal interface resistance and thermopower via grain boundary engineering in polycrystalline TE materials.

In this work, we employ a liquid interface-assisted hot deforming (HD) process to improve the TE performance of the commercial n-type Bi₂Te_{2.7}Se_{0.3} (BTS) matrix. KOH is used as the interface modification material, which could liquefy and flow along the grain boundaries of the BTS matrix during the HD process and results in the formation of an ultra-small grain size and highly distorted grain boundaries (Figure 1). By simulating the phonon/carrier transport properties using the two-phase model, it is found that the carrier/phonon segregation effect at the grain boundary could be increased by a factor of 3~7 for the sample after the HD process. As a result, a peak figure of merit $zT_{\rm max} \approx$ 1.22 at 425 K and an average $zT_{\text{avg}} \approx 1.1 \ (300-500 \ \text{K})$ are obtained in the optimized sample, which are about 55 and 57% higher than the corresponding values of the commercial BTS matrix, respectively. As shown in Figure 1a,b, compared with other recently reported n-type Bi₂Te₃-based high-performance TE materials, $^{13-20}$ the zT value obtained for this work is very competitive. Using the calculation method for conversion efficiency as described in ref 21, a high theoretical conversion efficiency of about 8.3% is achieved in the optimized material. 22,23 Moreover, considering the low cost and low toxicity of KOH as well as the use of the commercial BTS matrix material, the present grain boundary engineering

strategy possesses high industrial compatibility, a great commercial value, and enormous application potential.

2. EXPERIMENTAL SECTION

2.1. Materials Synthesis. The starting material for the experiment is the commercial n-type ZM BTS ingot purchased from Wangu Electronic Materials Co. The BTS/KOH samples with different KOH mass ratios are prepared by ball milling with zirconia balls at a milling speed of 800 rpm for 30 min in ambient Ar. The BTS/KOH samples with a KOH content of about 0.X wt % are noted as BKX. The bulk samples were obtained by hot pressing the obtained powers into cylinders in a φ 10 mm graphite die at 673 K for 30 min under the uniaxial stress of 60 MPa, named "HD1". The HD2 samples were obtained by hot-deforming the HD1 samples in a larger graphite die with an inner diameter of φ 11 mm at 673 K for 30 min. In the same way, the HD3 samples were obtained by hot-deforming the HD2 samples in a φ 12 mm graphite die. All the samples have a height of about 13 mm, making TE properties to be measured along the same directions. The square piece about 10 mm × 10 mm × 2 mm is first cut from the sintered pellets along the in-plane direction to measure the thermal diffusivity coefficient, and the cuboid sample about 3 mm \times 3 mm \times 10 mm is cut along the same direction to measure the σ and S.

2.2. Characterization. The X-ray powder diffraction (XRD) measurement is performed on a Bruker D8 Advance X-ray diffractometer; X-ray photoelectron spectroscopy (XPS) is performed on a Thermo Fisher ESCALAB 250X surface analysis system equipped with a monochromatized Al anode X-ray source ($h\nu=1486.6~{\rm eV}$). The overall morphology and detailed crystallographic information are deduced from high-resolution field-emission transmission electron microscopy (JEOL-3200FS, 300 kV). A focused ion beam system (JIB 4601F, JEOL) is used to prepare the TEM and electron backscatter diffraction (EBSD) samples of the sintered bulk.

2.3. Thermoelectric Measurements. The electrical conductivity and Seebeck coefficient are measured using a ULVAC ZEM-3 within the temperature range of 300–500 K. The total thermal conductivity

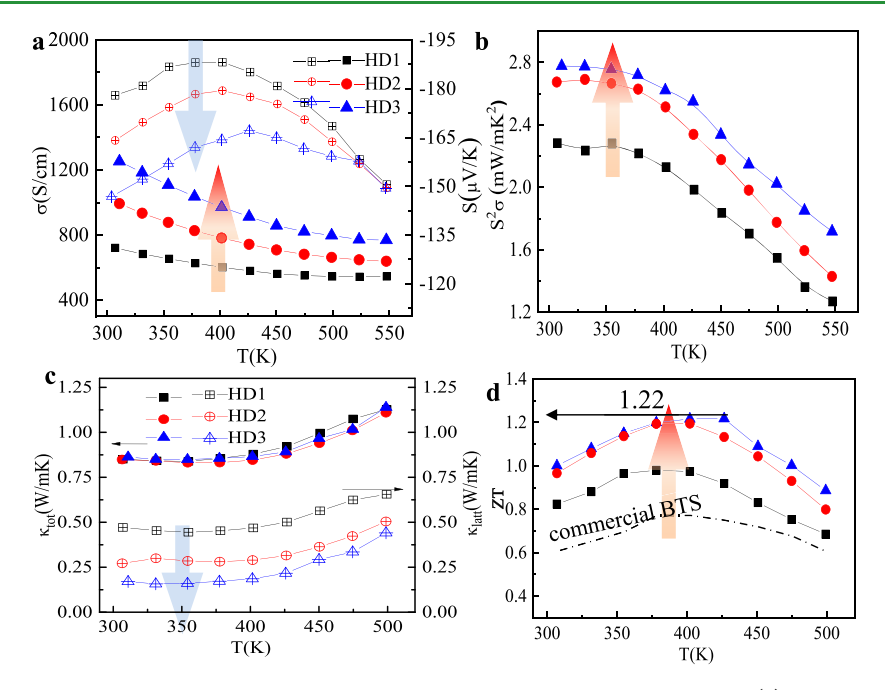


Figure 2. Thermoelectric properties of the as-prepared BK3 samples with different HD numbers. (a) Seebeck coefficient and electrical conductivity, (b) PF, (c) total thermal conductivity and lattice thermal conductivity, and (d) zT value.

 $(\kappa_{\rm tot})$ was calculated through $\kappa_{\rm tot}=DC_{\rm p}\rho$, where $D,\,C_{\rm p},$ and ρ are the thermal diffusivity coefficient, specific heat capacity, and density, respectively. The thermal diffusivity coefficient is measured using a laser flash apparatus using a Netzsch LFA 467 from 300 to 500 K, and the specific heat $(C_{\rm p})$ is tested using a differential scanning calorimeter (Mettler DSC1), and the density (ρ) is calculated by using the mass and dimension of the pellet.

3. RESULTS AND DISCUSSION

3.1. HD Process Enhances TE Performance. The HD process is employed to tune the grain size and the characteristics of the grain boundary in the nanocomposite samples. As described in the Experimental Section, pellets with different grain sizes are prepared via different HD numbers. Samples subjected to 1–3 HD processes are denoted as HD1–3, respectively. During the sintering process at 673 K, the KOH secondary phase became liquid and flowed along grain boundaries, which could be used to tune the grain size and the structural characteristics of the grain boundary. In the HD process, the deformation and fracture of BTS grains occurred and the liquid KOH phase flowed along the newly formed grain boundaries, which result in the significantly reduced grain size of the sample after the HD process, as shown in Figure 1c.d.

Figure 2 presents the typical TE transport properties of the samples subjected to different HD processes. It is found that with the increase of HD numbers, the overall TE property is gradually enhanced. Notably, all the samples exhibit a typical degenerate semiconductor behavior because the σ decreased monotonically with increasing temperature (Figure 2a). With the increased HD number, the σ increased significantly and the absolute value of S decreased. As a consequence, a significant improvement of power factor (PF) with the increased HD number is obtained. The highest PF achieved at 300 K for HD3 is about 2.79 mW/mK², which is about 22.4% higher than that of HD1 (2.28 mW/mK²). Correspondingly, the $\kappa_{\rm tot}$ value has no obvious change with the increased HD number, but $\kappa_{\rm latt}$ is significantly reduced (Figure 2c), which will be

discussed later with microstructure analysis and a two-phase model. The extremely low κ_{latt} of 0.17 W m⁻¹ K⁻¹ at 300 K is achieved in HD3, which decreased by approximately 60% compared with that of HD1. This is one of the lowest values comparable with reported values in the literature. 17,20,25 Consequently, the zT values are significantly improved after the HD process, reaching 1.22 at 425 K for HD3, which is one of the highest values of n-type Bi₂Te₃-based alloys reported in the literature. 17-20 The above results are different from that of the commercial BTS matrix after the HD process. As shown in Figure S1, after the HD process, the PF and κ_{tot} increased simultaneously, finally leading to a slight net enhancement of zT. It is obvious that the enhancement of zT for the commercial BTS matrix is related to the recrystallization during the HD process, which has been well studied by the previous reports. 15,24

To understand the carrier transport behaviors, the carrier concentration and mobility at 300 K are measured and analyzed. It is found that the values of carrier concentration and mobility are all increased with the increase of HD number (Table S1), which could be ascribed to the recrystallization during the HD process. The increased carrier concentration could be attributed to the increase of Te vacancies during the HD process, which induce the donor-like effect to the sample.²⁴ Although the carrier concentration increased after the HD process, the effective mass (m^*) is slightly increased, which is beneficial for the improvement of PF. As shown in Figure S2, m^* showed a slight enhancement with the increase of HD number mainly due to the increased carrier concentration. As a result, a large m^* and high charge carrier mobility could be achieved in the sample after the HD process. Such results indicate the effective improvement of the sample quality for charge carrier transport, 21 which is likely related to the optimized microstructure, such as the grain size, the thickness, and chemical components of grain boundaries.

3.2. Grain Size Variation during the HD Process. As described above, the grain size of the sample varies with the

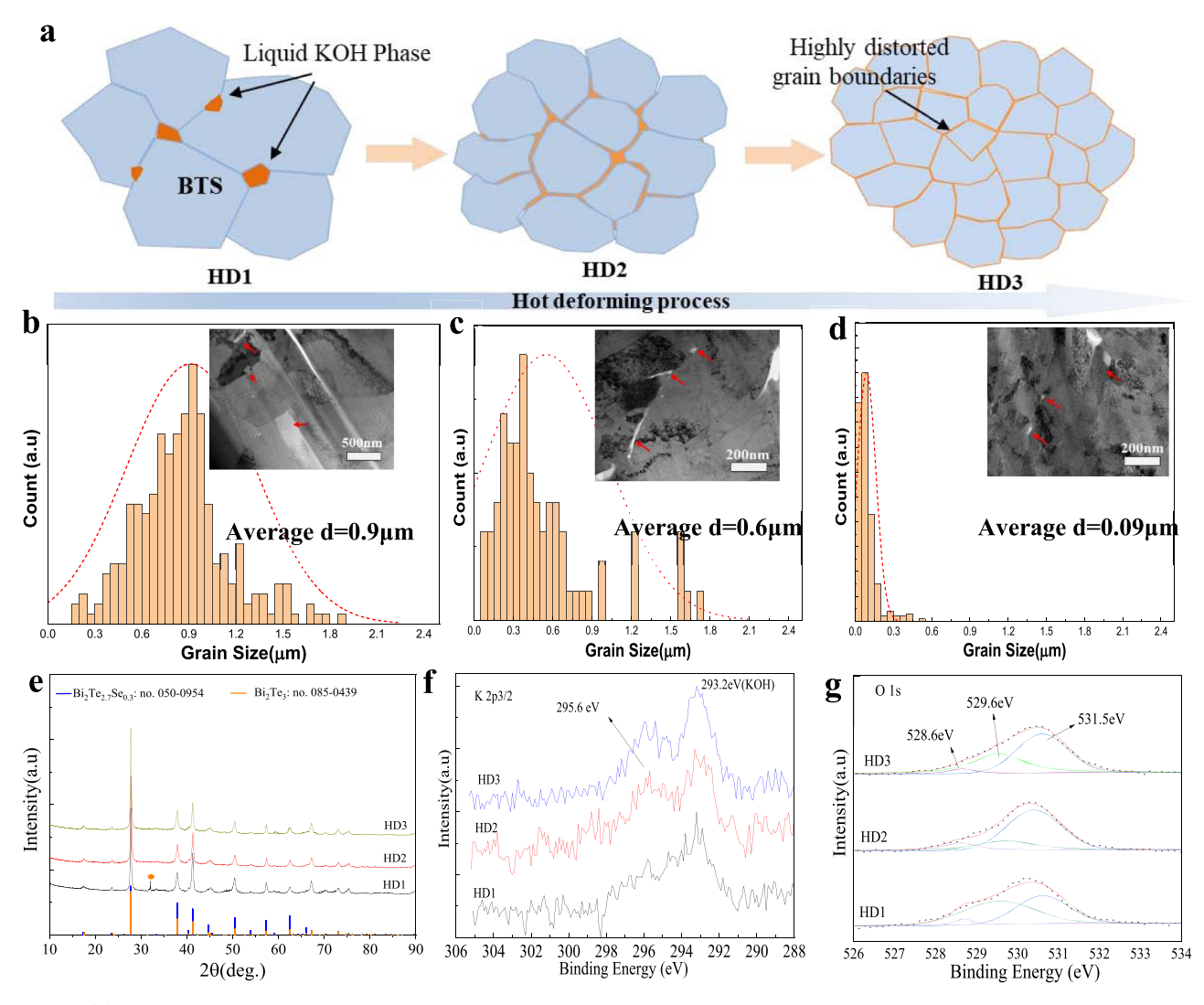


Figure 3. (a) Schematic diagrams of the liquid interface-assisted HD process. The size distribution determined by EBSD maps and the corresponding TEM images of the as-prepared (b) HD1, (c) HD2, and (d) HD3 samples. The XRD patterns and XPS spectra of the samples with different HD numbers. (e) XRD patterns, (f) K 2p peaks, and (g) O 1s peaks.

HD number, as present in the diagram in Figure 3a. According to the EBSD results, the grain size greatly reduced after the HD process. The grain size of the HD1 sample is about 900 nm, which is consistent with the values reported in the literature.8 After the HD process, the average grain size of the HD2 sample is greatly decreased to about 600 nm. After twice the HD process, the HD3 sample possesses a small average grain size of about 89 nm, presenting a decrease of 90% as compared to HD1. Besides, all the samples showed disordered crystallographic orientation, demonstrating that the grain growth could be effectively suppressed during the HD process due to the introduction of the liquid KOH phase. In addition to the grain size variation, distinct microstructure changes are also investigated by TEM (Figure S3). In the HD1 sample, the KOH phase is distributed as isolated patches between the large BTS grains, as noted in Figure S3a. Interestingly, the KOH phase distributed more uniformly at the grain boundaries in the HD2 sample. As for the HD3 sample, the obvious KOH phase almost disappeared and the high-density distorted grain boundaries can be clearly observed. These results confirmed that the liquid KOH phase flowed along the newly formed grain boundaries during the HD process.

3.3. Microstructure Evolution during the HD Process.

To examine the microstructure evolution during the HD process, XRD and XPS analysis are employed. As shown in Figure 3e, all the major diffraction peaks of the HD1 sample can be indexed to the $\mathrm{Bi_2Te_{2.7}Se_{0.3}}$ phase of standard JCPDS cards (no. 050-0954) with a rhombohedral crystal structure. It should be pointed out that the weak diffraction peaks from Bi₂Te₃ can be observed in the diffraction pattern of HD1 (JCPDS card no. 085-0439), which indicates the presence of a small proportion of the Bi₂Te₃ phase in the initial commercial materials.²⁶ Interestingly, after the HD process, the diffraction peaks from BT almost disappeared, which is likely related to the element diffusion under the high-temperature and highpressure conditions during the HD process. In order to further elucidate the composition of the samples, the chemical binding states of K and O ions are examined via XPS, as shown in Figure 3f,g. The K 2p region shows the K-OH peak at 293.2 eV originating from the added KOH phase. Moreover, in the sample after the HD process, a weak peak with a lower binding energy of 295.6 eV can be clearly observed, which may originate from the solid-phase diffusion of potassium ions from KOH to the BTS matrix. In the O 1s spectra, three peaks are observed, that is, the K-OH peak at 531.5 eV, the Bi-O peak at 529.6 eV, and the peak with a lower binding energy (528.6 eV) originating from oxygen atoms of the O-related dislocation clusters in the BTS matrix. According to the above results, it can be concluded that the liquid KOH phase can react with the BTS matrix during the HD process, which is the main reason for the formation of the highly distorted grain boundaries.

The detailed microstructural characterization of the HD3 sample after twice the HD process is performed by TEM, as shown in Figure 4. It reveals that the BTS grains with an

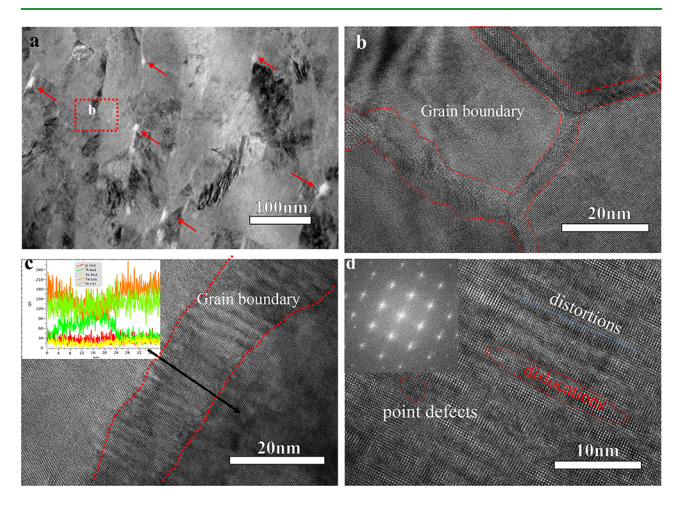


Figure 4. Microstructure of the as-prepared sample with a nanoscale grain size and highly distorted grain boundaries. (a) Low- and (b) high-magnification TEM images. (c,d) HRTEM images of highly distorted grain boundaries; the inset of (c) is the corresponding EDS line mapping and (d) FFT at highly distorted grain boundaries.

average size of about 100 nm are closely packed, which is in good agreement with the EBSD results. It is worth noting that KOH precipitates with the size in the range of 10-20 nm can be clearly observed at the BTS grain boundaries, as denoted by arrows (Figure 4a). Figure 4b shows the typical HRTEM image of two neighboring grains with uniform highly distorted grain boundaries. Most of the dislocations are found at grain boundaries instead of the inner part of grains, which is possibly due to the reaction between the liquid KOH phase and the BTS matrix as well as the generation of large strain at the grain boundaries during the HD process. Moreover, the magnified TEM image and the corresponding EDS line scans reflect that the highly distorted grain boundary is approximately 10-15 nm in thickness (Figure 4c), as revealed by enrichment of oxygen and potassium compared with the matrix regions. Figure 4d is the lattice image of distorted regions and the corresponding fast Fourier transform (FFT) image, which shows multiple sets of reflections with a close crystallographic relation. Various and abundant atomic scale distortions are unveiled, such as tiny distorted regions with distortions along the interfaces, dislocations, distorted layer interfaces, and the strain field domains. These atomic-scale distortions multiplied by various means play an important role in the scattering of mid-frequency phonons and also in the softening of the lattice, 23,27,28 which can effectively reduce the κ_{latt} . However, for electronic transport properties, the impacts from atomicscale distortions would be limited as compared to the secondphase precipitates.

3.4. Compositional Optimization of BTS/KOH. The TE properties of the as-prepared BTS/KOH HD1 samples are

shown in Figures 5 and S4. For the commercial BTS sample, the σ (~1075.9 S/cm) and S (-141.1 μ V/K) at 300 K are comparable to those of the reported Bi₂Te₃-based TE material.8 As shown in Figures 5a,b and S4a, due to the introduction of KOH, the σ value of as-prepared HD1 samples obviously decreased, and the absolute value of S increased remarkably. Typically, the PF value of BK3-HD1 was about 2.28 W m⁻¹ K⁻² at 300 K, which increased by approximately 7% compared with that of the BTS matrix (Figure 5c). As shown in Figures 5d and S5, compared with the $\kappa_{\rm tot}$ of the BTS matrix (~1.084Wm $^{-1}$ K $^{-1}$ at 300 K), the κ_{tot} of all the BK samples decreased due to the significant decrease of κ_{latt} . Moreover, the κ_{latt} decreased significantly with the increase of KOH content and tended to saturate with a high KOH content (>0.3 wt %). Finally, the maximum zT value of 0.98 at 375 K was obtained for BK3-HD1, presenting an increase of $\approx 27.3\%$ as compared with the commercial BTS matrix.

The TE properties of the samples could be further enhanced by the HD process. For the sample after different HD numbers, the σ decreased with the increase of KOH content (Figure S6 and Figure S7). For all samples, the σ increased significantly with the increase of HD number, as shown in Figure 5a. Notably, the improvement of σ can be attributed to the above-mentioned element diffusion as well as the elimination of defects in the grains due to high temperature. As depicted in Figure 5b, the absolute value of S exhibited an increasing trend with the increase of KOH content for the samples with different HD numbers. As the HD number increased, the absolute value of S decreased due to the improvement of σ . Obviously, with the increase in HD number, the decrements of the absolute value of *S* are found to be proportionately lower compared with the increments of σ , resulting in the significantly improved PF (Figure 5c). The highest PF achieved for BK3-HD3 is 2.79 mW/mK², which is about 22.4 and 30.4% higher than that of BK3-HD1 and the BTS matrix, respectively. It is worth noting that the PF values obtained in the present work are at very high levels as compared with those of other recent works that are reported concerning the high performance of n-type Bi₂Te₃-based TE materials. 8,18,19,23 The thermal transport properties are also found to be effectively modulated by the HD process, as shown in Figure 5d,e. The κ_{tot} increased significantly with the increase of HD number for the samples with low KOH contents (<0.3 wt %) (Figure S8 and Figure S9). However, for the samples with high KOH contents (>0.3 wt %), the κ_{tot} increased slightly with the increase of the HD number. In particular, the κ_{tot} at 300 K of BK3-HD1 was 0.85 W m⁻¹ K⁻¹, which only increased to 0.86Wm⁻¹ K⁻¹ for BK3-HD3. Correspondingly, the increasing of κ_{tot} with the increase of HD number is mainly due to the increased σ , and the κ_{latt} is significantly reduced. The extremely low κ_{latt} of 0.17 W m⁻¹ K⁻¹ at 300 K was achieved for BK3-HD3, which decreased by approximately 70% compared with that of BK3-HD1. The massively increased grain boundary density, originating from the decrease of the grain size from 900 to 89 nm due to the HD process, is the main reason for the reduction of κ_{latt} . Moreover, the increased interfacial thermal resistance of highly distorted grain boundaries also contributes to the extremely low $\kappa_{\text{latt.}}$ which will be discussed below. As presented in Figure 5f, the zT values greatly increased after the HD process. The highest zT of about 1.22 at 425 K could be obtained for the BK3-HD3 sample, which is twice as high as that of the commercial BTS matrix. Our work employed a combined liquid-phase sintering

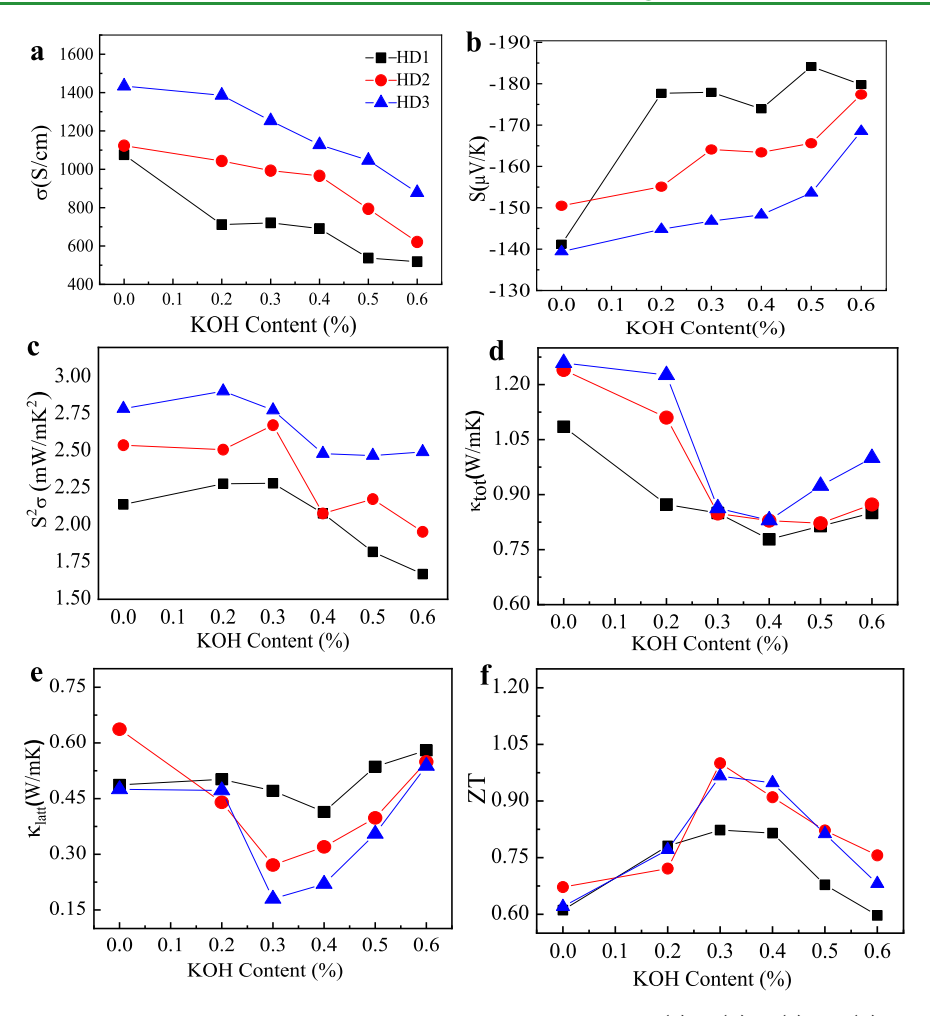


Figure 5. Thermoelectric properties at 300 K of the as-prepared BK samples. The variations of (a) σ , (b) S, (c) PF, (d) κ_{tov} (e) κ_{latv} and (f) zT as a function of the KOH content at 300 K for the BK samples.

and HD technique to construct the highly distorted grain boundaries with an enhanced carrier/phonon segregation effect, which successfully increased the zT of the commercial n-type $\mathrm{Bi_2Te_{2.7}Se_{0.3}}$ matrix to one of the highest reported values for n-type $\mathrm{Bi_2Te_3}$ alloys. 8,18,19,23

3.5. Effects of Grain Boundaries to the Phonon/ Carrier Transport Behaviors. It is should be noted that in a bulk TE material with abundant grain boundaries, the carrier/ phonon transport behaviors in grains and at grain boundaries are different. 29-31 For the carrier transport, the potential barrier at the grain boundary may lead to a larger magnitude of the Seebeck coefficient as well as an interfacial resistance due to the energy filtering effect (Figure 6a). On the other hand, due to the extra phonon scattering centers at the grain boundaries, additional interfacial thermal resistance (Kapitza resistance) could be introduced.³² The two-phase model consisting of the grain phase and grain boundary phase is usually adopted to analysis of the transport behaviors of the carrier/phonon in the bulk TE material with charged grain boundaries.³³ Thus, the two-phase model is used to simulate and explain the Seebeck coefficient, thermal conductivity, and electrical conductivity of the as-prepared samples made up of BTS grains and highly distorted grain boundaries. In this work, with the increased HD number, the fractional amount of the grain boundary "phase" increased due to the decreased grain size. Moreover, by tuning the KOH content, the interfacial

thermal resistance ($\kappa_{\rm Kapitza}$) and interfacial electrical resistance ($\rho_{\rm ad-gb}$) at the grain boundaries could be optimized, which is crucial to enhancing the TE performance of the samples. Based on previous research, ^{33–36} the two-phase model is used to simulate and explain the phonon/carrier transport behaviors of the as-prepared samples. In this model, the phonon/carrier transport contains contributions from the initial BTS matrix and an additional contribution from the highly distorted grain boundary. For the electron transport, the total electric resistance is a sum of electric resistance in the pure BTS sample and the additional electric resistance at the highly distorted grain boundary. For a material with average grain size d, the electric conductivity could be expressed as

$$\frac{d}{\sigma_{\text{tot}}} = \frac{d}{\sigma_{\text{BTS}}} + \rho_{\text{ad-gb}}$$

where $\sigma_{\rm tot}$ and $\sigma_{\rm BTS}$ are the electrical conductivities of the asprepared samples and pure BTS, respectively, and $\rho_{\rm ad\text{-}gb}$ is the additional interfacial electrical resistance originating from the highly distorted grain boundary. Here, the average grain size d of the sample can be determined by EBSD results. In the same way, the $\kappa_{\rm tot}$ could be expressed as

$$\frac{d}{\kappa_{\text{tot}}} = \frac{d}{\kappa_{\text{BTS}}} + \kappa_{\text{Kapitz}}$$

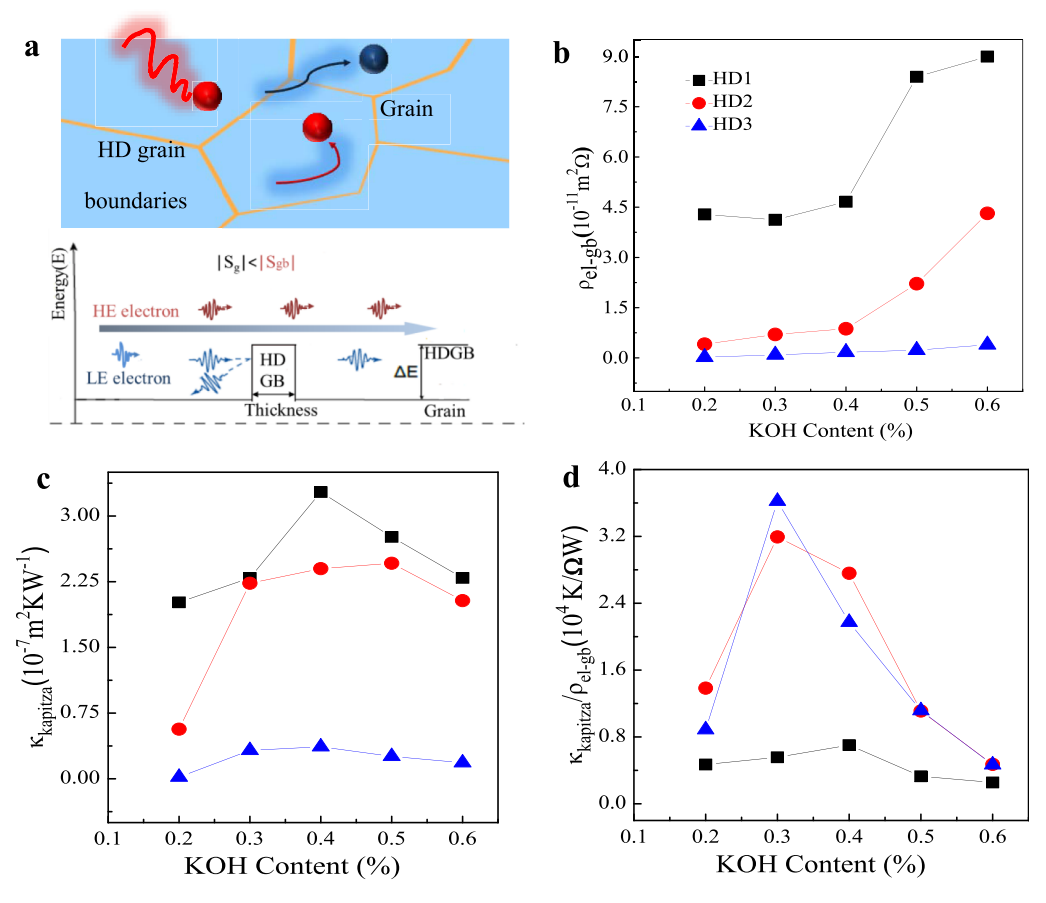


Figure 6. (a) Illustration of the energy filtering effect in the as-prepared samples with highly distorted grain boundaries. Analysis of BK samples with different KOH contents and different HD numbers using the two-phase model. (b) Interfacial electrical resistance ($\rho_{\text{el-gb}}$), (c) interfacial thermal resistance (κ_{Kapitza}), and (d) value of κ_{Kapitza} / $\rho_{\text{el-gb}}$ at 300 K of the as-prepared BK samples.

where $\kappa_{\rm tot}$ and $\kappa_{\rm BTS}$ are the thermal conductivities of the asprepared samples and pure BTS, respectively, and $\kappa_{\rm Kapitza}$ is the additional interfacial thermal resistance.³³ Meanwhile, the additional Seebeck coefficient ($S_{\rm gb}$) could also be estimated according the formula

$$S_{\text{tot}} = \frac{(S_{\text{BTS}} - S_{\text{gb}})\kappa_{\text{tot}}}{\kappa_{\text{BTS}}} + S_{\text{gb}}$$

where $S_{\rm tot}$ and $S_{\rm gb}$ represent the apparent overall Seebeck coefficient and the additional Seebeck coefficient ($S_{\rm gb}$) originating from the highly distorted grain boundary, respectively.

3.6. Enhanced Carrier/Phonon Segregation Effect at Highly Distorted Grain Boundaries. According to above two-phase model, the κ_{Kapitza} , $\rho_{\text{ad-gb}}$, and S_{gb} of the as-prepared samples could be obtained, as present in Figures 6 and \$10. It is found that for all the samples, the absolute values of S_{gb} are larger than that of the bulk Seebeck coefficient due to the energy filtering effect at the grain boundaries. In particular, the absolute value of S_{gb} for HD1 samples is about 256.9~328, which almost 3 times larger than that of the pure BTS bulk. Obviously, with the increase of the HD number, the absolute value of S_{gb} decreased significantly, which suggests that the energy offset of the electron filtering barrier could be influenced by the HD process. As shown in Figure 6b, the $\rho_{\text{ad-gb}}$ at 300 K for the samples after the HD process are estimated. It is obvious that the $\rho_{\text{ad-gb}}$ increased significantly with the increase of the KOH content, which is consistent with

the decreased σ . Compared to the HD1 samples, the $\rho_{\text{ad-gb}}$ decreased by a factor of 20-40 after the HD process. Typically, the $\rho_{\rm ad-gb}$ is about 4.1 \times 10⁻¹¹ m² Ω for BK3-HD1, which is nearly 40 times greater than that of BK3-HD3 $(0.09 \times 10^{-11} \,\mathrm{m}^2 \,\Omega)$. This observation suggests that the energy offset of the electron filtering barrier at a highly distorted grain boundary could be influenced by the HD process. Decreasing the thickness of the grain boundary layer due to the flow of liquid KOH as well as reducing their resistance are two potential explanations for the huge reduction of $\rho_{\rm ad\text{-}gb}$ after the HD process. In the same way, the $\kappa_{\mathrm{Kapitza}}$ could be estimated, as shown in Figure 6c. Corresponding to the $ho_{
m ad-gb}$, the $\kappa_{
m Kapitza}$ decreased by a factor of 5-10 after the HD process. Thus, in this work, the HD process results in the simultaneously decreased $ho_{ ext{ad-gb}}$ and $\kappa_{ ext{Kapitza}}$, mainly due to the reduced thickness of the grain boundary phase as well as the changed energy offset of the electron filtering barrier.

The core idea of the grain boundary engineering is to modify grain boundaries in order to reduce κ without detriment to σ by taking into account difference of scattering lengths of carriers and phonons, which requires larger $\kappa_{\rm Kapitza}$ and small $\rho_{\rm ad-gb}$ values simultaneously. Thus, the value of $\kappa_{\rm Kapitza}/\rho_{\rm ad-gb}$ is used to estimate the benefit of the grain boundary phase to the separation of the carrier and phonon. As shown in Figure 6d, after the HD process, the value of $\kappa_{\rm Kapitza}/\rho_{\rm ad-gb}$ increased by a factor of 3–7 compared to that of the HD1 sample, which finally contributes to the enhanced TE performance.

3.7. Grain Boundary Engineering Enhanced TE Performance. In this paper, we propose KOH liquid-assisted grain boundary engineering to improve the TE performance of the commercial n-type Bi₂Te_{2.7}Se_{0.3} matrix. In the as-prepared sample, highly distorted grain boundaries with the enhanced carrier/phonon segregation effect could be introduced to optimize the phonon/carrier transport behaviors. For the electrical transport properties, the energy filtering effect is related the potential barrier height as well as the barrier thickness at the grain boundary, which can be adjusted by tuning the KOH content and HD number. Obviously, with the increase of KOH content, the thickness of the grain boundary layer increased, which is in accord with the results that $\rho_{\mathrm{ad-eb}}$ and κ_{Kapitza} increased significantly with the increase of the KOH content. On the contrary, because the liquid KOH phase flowed along grain boundaries, the thickness of the grain boundary layer could be decreased significantly with the increase of the HD number, which results in the decreased $ho_{ ext{ad-gb}}$ and $\kappa_{ ext{Kapitza}}$. Moreover, the potential barrier height may also be changed after the HD process due to the abovementioned element diffusion as well as the elimination of defects in the grains. Thus, by regulating the thickness and height of the potential barrier at the grain boundary, the carrier transport properties could be optimized by energy filtering effects.

According to the Callaway model, various phonon-scattering mechanisms contribute to the reduced thermal conductivity, including phonon-phonon Umklapp scattering, grain boundary scattering, point defect scattering, and nanoprecipitate scattering. ^{23,37–39} Usually, grain boundaries are considered as 2D defects, which scattered phonons at low frequencies. For the as-prepared samples with the highly distorted grain boundaries, the grain interface, point defect, and nanoprecipitate can scatter phonons over the entire frequency range and largely decreased the κ_{latt} . Thus, compared with the conventional grain boundary, the κ_{Kapitza} of the highly distorted grain boundaries is significantly increased. Moreover, according to the previous report, the special structure that the grains surrounded by the coating layer offers much larger phononscattering cross-sections compared to those of nanocomposites, which may also contribute to the low κ_{latt} of as-prepared samples. As can be seen, due to the enhanced carrier/phonon segregation effect at the highly distorted grain boundary, our work presents excellent commercial Bi₂Te_{2.7}Se_{0.3} TE materials with high performance.

4. CONCLUSIONS

In conclusion, a highly distorted grain boundary with enhanced carrier/phonon segregation effect is introduced to the BTS TE materials by the liquid-phase sintering-assisted HD technique. KOH is used as the interface modification material, which could liquefy and flow along the grain boundaries of the BTS matrix during the HD process and results in the formation of an ultra-small grain size and highly distorted grain boundaries. The calculation reveals that the carrier/phonon segregation effect at the grain boundary could be increased by a factor of 3-7 for the sample after the HD process. The total effect is the enhancement of the zT value to the highest 1.22 at 425 K, which is about 55% higher compared to the value of the commercial n-type Bi₂Te_{2.7}Se_{0.3} matrix. A high theoretical conversion efficiency of about 8.3% is achieved in the asprepared material, which is about 38% higher than that of the reported ZM sample. Moreover, considering the low cost and

low toxicity of KOH as well as use of the commercial BTS matrix material, the present strategy has high industrial compatibility, a great commercial value, and enormous application potential.

ASSOCIATED CONTENT

Solution Supporting Information

The Supporting Information is available free of charge at https://pubs.acs.org/doi/10.1021/acsami.1c15422.

Details on powder XRD, scanning electron microscopy, and TE measurements (PDF)

AUTHOR INFORMATION

Corresponding Authors

Yinguo Xiao — School of Advanced Materials, Peking University Shenzhen Graduate School, Shenzhen 518055, China; orcid.org/0000-0001-9306-908X; Email: y.xiao@pku.edu.cn

Feng Pan — School of Advanced Materials, Peking University Shenzhen Graduate School, Shenzhen 518055, China; orcid.org/0000-0002-8216-1339; Email: panfeng@pkusz.edu.cn

Authors

Shuankui Li — School of Advanced Materials, Peking University Shenzhen Graduate School, Shenzhen 518055, China

Zhongyuan Huang — School of Advanced Materials, Peking University Shenzhen Graduate School, Shenzhen 518055, China

Rui Wang — School of Advanced Materials, Peking University Shenzhen Graduate School, Shenzhen 518055, China

Wenguang Zhao – School of Advanced Materials, Peking University Shenzhen Graduate School, Shenzhen 518055, China

Jun Luo — School of Materials Science and Engineering, Shanghai University, Shanghai 200444, China; orcid.org/0000-0002-8235-2338

Complete contact information is available at: https://pubs.acs.org/10.1021/acsami.1c15422

Funding

This work was financially supported by the National Natural Science Foundation of China (no. 21905007) and the Soft Science Research Project of Guangdong Province (no. 2017B030301013).

Notes

The authors declare no competing financial interest.

REFERENCES

- (1) Bahrami, A.; Schierning, G.; Nielsch, K. Waste Recycling in Thermoelectric Materials. *Adv. Energy Mater.* **2020**, *10*, 1904159.
- (2) Choi, H.; Kim, Y. J.; Song, J.; Kim, C. S.; Lee, G. S.; Kim, S.; Park, J.; Yim, S. H.; Park, S. H.; Hwang, H. R.; Hong, M. H.; Veluswamy, P.; Cho, B. J. UV-Curable Silver Electrode for Screen-Printed Thermoelectric Generator. *Adv. Funct. Mater.* **2019**, 29, 1901505.
- (3) Poudel, B.; Hao, Q.; Ma, Y.; Lan, Y.; Minnich, A.; Yu, B.; Yan, X.; Wang, D.; Muto, A.; Vashaee, D.; Chen, X.; Liu, J.; Dresselhaus, M. S.; Chen, G.; Ren, Z. High-Thermoelectric Performance of Nanostructured Bismuth Antimony Telluride Bulk Alloys. *Science* **2008**, *320*, 634–638.

- (4) Wang, T.; Zhang, C.; Snoussi, H.; Zhang, G. Machine Learning Approaches for Thermoelectric Materials Research. *Adv. Funct. Mater.* **2020**, *30*, 1906041.
- (5) Li, S.; Chu, M.; Zhu, W.; Wang, R.; Wang, Q.; Liu, F.; Gu, M.; Xiao, Y.; Pan, F. Atomic-scale Tuning of Oxygen-doped Bi₂Te_{2.7}Se_{0.3} to Simultaneously Enhance the Seebeck Coefficient and Electrical Conductivity. *Nanoscale* **2020**, *12*, 1580–1588.
- (6) Sugahara, T.; Ekubaru, Y.; Nong, N. V.; Kagami, N.; Ohata, K.; Hung, L. T.; Okajima, M.; Nambu, S.; Suganuma, K. Fabrication with Semiconductor Packaging Technologies and Characterization of a Large-Scale Flexible Thermoelectric Module. *Adv. Mater. Technol.* **2019**, *4*, 1800556.
- (7) Xiao, C.; Li, Z.; Li, K.; Huang, P.; Xie, Y. Decoupling Interrelated Parameters for Designing High Performance Thermoelectric Materials. *Acc. Chem. Res.* **2014**, *47*, 1287–1295.
- (8) Li, S.; Huang, Z.; Wang, R.; Wang, C.; Zhao, W.; Yang, N.; Liu, F.; Luo, J.; Xiao, Y.; Pan, F. Precision Grain Boundary Engineering in Commercial Bi₂Te_{2.7}Se_{0.3} Thermoelectric Materials towards High Performance. *J. Mater. Chem. A* **2021**, *9*, 11442–11449.
- (9) Kuo, J. J.; Kang, S. D.; Imasato, K.; Tamaki, H.; Ohno, S.; Kanno, T.; Snyder, G. J. Grain Boundary Dominated Charge Transport in Mg₃Sb₂-based Compounds. *Energy Environ. Sci.* **2018**, 11, 429–434.
- (10) Pike, G. E.; Seager, C. H. The dc voltage dependence of semiconductor grain-boundary resistance. *J. Appl. Phys.* **1979**, *50*, 3414–3422.
- (11) Mataré, H. F. Carrier Transport at Grain Boundaries in Semiconductors. *J. Appl. Phys.* **1984**, *56*, 2605–2631.
- (12) Hu, Y.; Li, S.; Bao, H. First-principles Based Analysis of Thermal Transport in Metallic Nanostructures: Size Effect and Wiedemann-Franz Law. *Phys. Rev. B* **2021**, *103*, 104301.
- (13) Chen, B.; Li, J.; Wu, M.; Hu, L.; Liu, F.; Ao, W.; Li, Y.; Xie, H.; Zhang, C. Simultaneous Enhancement of the Thermoelectric and Mechanical Performance in One-Step Sintered n-Type Bi₂Te₃-Based Alloys via a Facile MgB₂ Doping Strategy. *ACS Appl. Mater. Interfaces* **2019**, *11*, 45746–45754.
- (14) Cho, H.; Yun, J. H.; Kim, J. H.; Back, S. Y.; Lee, H. S.; Kim, S. J.; Byeon, S.; Jin, H.; Rhyee, J.-S. Thermoelectric Properties and Low-Energy Carrier Filtering by Mo Microparticle Dispersion in an n-Type (CuI)_{0.003}Bi₂(Te,Se)₃ Bulk Matrix. ACS Appl. Mater. Interfaces **2020**, 12, 925–933.
- (15) Hu, L.; Wu, H.; Zhu, T.; Fu, C.; He, J.; Ying, P.; Zhao, X. Tuning Multiscale Microstructures to Enhance Thermoelectric Performance of n-type Bismuth-Telluride-based Solid Solutions. *Adv. Energy Mater.* **2015**, *5*, 1500411.
- (16) Nozariasbmarz, A.; Poudel, B.; Li, W.; Kang, H. B.; Zhu, H.; Priya, S. Bismuth Telluride Thermoelectrics with 8% Module Efficiency for Waste Heat Recovery Application. *iScience* **2020**, 23, 101340.
- (17) Xu, B.; Feng, T.; Agne, M. T.; Zhou, L.; Ruan, X.; Snyder, G. J.; Wu, Y. Highly Porous Thermoelectric Nanocomposites with Low Thermal Conductivity and High Figure of Merit from Large-Scale Solution-Synthesized Bi₂Te_{2.5}Se_{0.5} Hollow Nanostructures. *Angew. Chem., Int. Ed.* **2017**, *56*, 3546–3551.
- (18) Li, S.; Wang, R.; Zhu, W.; Chu, M.; Huang, Z.; Zhang, Y.; Zhao, W.; Liu, F.; Luo, J.; Xiao, Y.; Pan, F. Achieving High Thermoelectric Performance by Introducing 3D Atomically Thin Conductive Framework in Porous Bi₂Te_{2.7}Se_{0.3}-Carbon Nanotube Hybrids. *Adv. Electron. Mater.* **2020**, *6*, 2000292.
- (19) Li, S.; Liu, X.; Liu, Y.; Liu, F.; Luo, J.; Pan, F. Optimized Hetero-interfaces by Tuning 2D SnS₂ Thickness in Bi₂Te_{2.7}Se_{0.3}/SnS₂ Nanocomposites to Enhance Thermoelectric Performance. *Nano Energy* **2017**, *39*, 297–305.
- (20) Li, S.; Xin, C.; Liu, X.; Feng, Y.; Liu, Y.; Zheng, J.; Liu, F.; Huang, Q.; Qiu, Y.; He, J.; Luo, J.; Pan, F. Effective Atomic Interface Engineering in Bi₂Te_{2.7}Se_{0.3} Thermoelectric Material by Atomic-Layer-Deposition Approach. *Nano Energy* **2016**, *30*, 780–789.

- (21) Snyder, G. J.; Snyder, A. H. Figure of Merit ZT of a Thermoelectric Device Defined from Materials Properties. *Energy Environ. Sci.* **2017**, *10*, 2280.
- (22) Yang, G.; Niu, R.; Sang, L.; Liao, X.; Mitchell, D. R. G.; Ye, N.; Pei, J.; Li, J. F.; Wang, X. Thermoelectrics: Ultra-High Thermoelectric Performance in Bulk BiSbTe/Amorphous Boron Composites with Nano-Defect Architectures (Adv. Energy Mater. 41/2020). Adv. Energy Mater. 2020, 10, 2070171.
- (23) Zhu, B.; Liu, X.; Wang, Q.; Qiu, Y.; Shu, Z.; Guo, Z.; Tong, Y.; Cui, J.; Gu, M.; He, J. Realizing Record High Performance in n-type Bi₂Te₃-based Thermoelectric Materials. *Energy Environ. Sci.* **2020**, *13*, 2106–2114.
- (24) Xiong, C.; Shi, F.; Wang, H.; Cai, J.; Zhao, S.; Tan, X.; Hu, H.; Liu, G.; Noudem, J. G.; Jiang, J. Achieving High Thermoelectric Performance of n-Type Bi₂Te_{2.79}Se_{0.21} Sintered Materials by Hot-Stacked Deformation. *ACS Appl. Mater. Interfaces* **2021**, *13*, 15429–15436.
- (25) Choi, H.; Jeong, K.; Chae, J.; Park, H.; Baeck, J.; Kim, T. H.; Song, J. Y.; Park, J.; Jeong, K.-H.; Cho, M.-H. Enhancement in Thermoelectric Properties of Te-embedded Bi₂Te₃ by Preferential Phonon Scattering in Heterostructure Interface. *Nano Energy* **2018**, 47, 374–384.
- (26) Jabar, B.; Qin, X.; Li, D.; Zhang, J.; Mansoor, A.; Xin, H.; Song, C.; Huang, L. Achieving High Thermoelectric Performance through Constructing Coherent Interfaces and Building Interface Potential Barriers in n-type Bi₂Te₃/Bi₂Te_{2.7}Se_{0.3} Nanocomposites. *J. Mater. Chem. A* **2019**, *7*, 19120–19129.
- (27) Novak, T. G.; Kim, K.; Jeon, S. 2D and 3D Nanostructuring Strategies for Thermoelectric Materials. *Nanoscale* **2019**, *11*, 19684–19699.
- (28) Chen, G. Thermal Conductivity and Ballistic-Phonon Transport in the Cross-plane Direction of Superlattices. *Phys. Rev. B* **1998**, 57, 14958–14973.
- (29) Kuo, J. J.; Wood, M.; Slade, T. J.; Kanatzidis, M. G.; Snyder, G. J. Systematic Over-Estimation of Lattice Thermal Conductivity in Materials with Electrically-Resistive Grain Boundaries. *Energy Environ. Sci.* **2020**, *13*, 1250–1258.
- (30) Cantwell, P. R.; Tang, M.; Dillon, S. J.; Luo, J.; Rohrer, G. S.; Harmer, M. P. Grain Boundary Complexions. *Acta Mater.* **2014**, *62*, 1–48.
- (31) Bergman, D. J.; Levy, O. Thermoelectric Properties of a Composite Medium. J. Appl. Phys. 1991, 70, 6821–6833.
- (32) Nan, C.-W.; Birringer, R.; Clarke, D. R.; Gleiter, H. Effective Thermal Conductivity of Particulate Composites with Interfacial Thermal Resistance. *J. Appl. Phys.* **1997**, *81*, 6692–6699.
- (33) Lin, Y.; Wood, M.; Imasato, K.; Kuo, J. J.; Lam, D.; Mortazavi, A. N.; Slade, T. J.; Hodge, S. A.; Xi, K.; Kanatzidis, M. G.; Clarke, D. R.; Hersam, M. C.; Snyder, G. J. Expression of Interfacial Seebeck Coefficient through Grain Boundary Engineering with Multi-layer Graphene Nanoplatelets. *Energy Environ. Sci.* **2020**, *13*, 4114–4121.
- (34) Kuo, J. J.; Kang, S. D.; Imasato, K.; Tamaki, H.; Ohno, S.; Kanno, T.; Snyder, G. J. Grain Boundary Dominated Charge Transport in Mg₃Sb₂-based Compounds. *Energy Environ. Sci.* **2018**, *11*, 429.
- (35) Bergman, D. J.; Levy, O. Thermoelectric Properties of a Composite Medium. J. Appl. Phys. 1991, 70, 6821–6833.
- (36) Mclachlan, D. S.; Blaszkiewicz, M.; Newnham, R. E. Electrical Resistivity of Composites. *J. Am. Ceram. Soc.* **1990**, *73*, 2187–2203.
- (37) Pan, Y.; Qiu, Y.; Witting, I.; Zhang, L.; Fu, C.; Li, J.-W.; Huang, Y.; Sun, F.-H.; He, J.; Snyder, G. J.; Felser, C.; Li, J.-F. Synergistic Modulation of Mobility and Thermal Conductivity in (Bi,Sb)₂Te₃ towards High Thermoelectric Performance. *Energy Environ. Sci.* **2019**, 12, 624–630.
- (38) Zeier, W. G.; Zevalkink, A.; Gibbs, Z. M.; Hautier, G.; Kanatzidis, M. G.; Snyder, G. J. Thinking Like a Chemist: Intuition in Thermoelectric Materials. *Angew. Chem., Int. Ed.* **2016**, *55*, 6826–6841.

(39) Kim, H.-S.; Kang, S. D.; Tang, Y.; Hanus, R.; Jeffrey Snyder, G. Dislocation Strain as the Mechanism of Phonon Scattering at Grain Boundaries. *Mater. Horiz.* **2016**, *3*, 234–240.